



1 **A CONCEPTUAL MODEL-BASED SEDIMENT CONNECTIVITY ASSESSMENT FOR**
2 **PATCHY AGRICULTURAL CATCHMENTS**

3 Pedro V. G. Batista^{1*}, Peter Fiener², Simon Scheper¹, Christine Alewell¹

4 ¹Department of Environmental Sciences, Universität Basel, Bernoullistrasse 30, 4056, Basel,
5 Switzerland.

6 ²Institute for Geography, Universität Augsburg, Alter Postweg 118, D – 86159, Augsburg, Germany.

7 *pedro.batista@unibas.ch

8



9 **ABSTRACT**

10 The accelerated sediment supply from agricultural soils to riverine and lacustrine environments leads to
11 negative off-site consequences. In particular, the sediment connectivity from agricultural land to surface
12 waters is strongly affected by landscape patchiness and the linear structures that separate field parcels
13 (e.g. roads, tracks, hedges, and grass-buffer-strips). Understanding the feedbacks between these
14 structures and sediment transfer is therefore crucial for minimising off-site erosion impacts. Although
15 soil erosion models can be used to understand lateral sediment transport patterns, model-based
16 connectivity assessments are hindered by the uncertainty in model structures and input data. In
17 particular, the representation of linear landscape features in numerical soil redistribution models is often
18 compromised by the spatial resolution of the input data and the quality of the process descriptions. Here
19 we adapted the WaTEM/SEDEM model using high resolution spatial data (2 m x 2 m) to analyse the
20 sediment connectivity in a very patchy mesoscale catchment (73 km²) of the Swiss Plateau. Specifically,
21 we used a global sensitivity analysis to explore model structural assumptions about how linear landscape
22 features (dis)connect the sediment cascade. Furthermore, we compared model simulations of hillslope
23 sediment yields from five sub-catchments to tributary sediment loads, which were calculated with long-
24 term water discharge and suspended sediment measurements. Our results showed that roads were the
25 main regulators of sediment connectivity in the catchment. In particular, the sensitivity analysis revealed
26 that the assumptions about how the road network (dis)connects the sediment transfer from field-blocks
27 to water courses had a much higher impact on modelled sediment yields than the uncertainty in model
28 parameters. Moreover, model simulations showed a higher agreement with tributary sediment loads
29 when the road network was assumed to directly connect sediments from hillslopes to water courses. Our
30 results ultimately illustrate how a high-density road network combined with an effective drainage system
31 increase sediment connectivity from hillslopes to surface waters in this representative catchment of the
32 Swiss Plateau. This further highlights the importance of considering linear structures in soil erosion and
33 sediment connectivity models.

34



35 **1 INTRODUCTION**

36 Rainfall events on sloped surfaces continuously displace small amounts of soil, which are transported
37 downslope as sediments. These sediments are then stored and remobilised several times before
38 conceivably reaching surface waters. Accordingly, the sediment cascade is a natural and potentially long
39 geomorphological process (Fryirs, 2013). However, the accelerated sediment supply from agricultural
40 soils to riverine and lacustrine environments leads to negative off-site consequences. Specifically,
41 nutrient-rich and pollutant-bound particulate matter from arable land is associated to the eutrophication
42 and contamination of water courses (Krasa et al., 2019; Laceby et al., 2021). Extreme erosion events in
43 agricultural fields are also linked to the occurrence of muddy floods (Boardman, 2020) and to damages
44 to downstream infra-structure (Bauer et al., 2019). Therefore, understanding how and when sediment is
45 transferred from agricultural fields to different landscape compartments is imperative to reduce off-site
46 erosion impacts.

47 The degree with which a system facilitates sediment transfer within its internal compartments is defined
48 by Heckmann et al. (2018) as sediment connectivity. This concept can be further distinguished into a
49 structural component, associated to the semi-static spatial configuration of the landscape; and a
50 functional one, which emerges as a dynamic property of the hydro-sedimentological system
51 (Wainwright et al., 2011). Connectivity theory therefore provides a framework to rethink the sediment
52 delivery problem (Fryirs, 2013; Parsons et al., 2009) and to understand the complex spatio-temporal
53 processes that regulate sediment transport.

54 In agricultural landscapes, sediment connectivity is strongly affected by the patchiness of the land use
55 configuration, and the presence of linear features between field parcels (e.g. hedges, grass-buffer-strips,
56 and roads) (Alder et al., 2015; Bakker et al., 2008; Chartin et al., 2013; Fiener et al., 2011; Van Oost et
57 al., 2000). The importance of landscape patchiness in regulating sediment transfer is specifically relevant
58 in areas where a large number of small fields, separated by linear structures, create a complex
59 hydrological system. However, the experimental analysis of sediment connectivity at catchment scale is
60 challenging, as it involves measuring both internal soil redistribution processes and cascading sediment
61 transport rates. The interaction between landscape patchiness, linear structures, and sediment
62 connectivity is therefore not addressed by the typical setup of experimental erosion studies, which either
63 focus on small erosion plots or catchment sediment yields (Fiener et al., 2019).

64 Due to the difficulties in measuring the processes that affect sediment movement at catchment and
65 landscape scale, it is common practice to analyse connectivity with modelling approaches (Nunes et al.,
66 2018). These usually rely on high-resolution process-based models, assuming they are able to explicitly
67 take connectivity into account (Baartman et al., 2020); semi-qualitative indices (Borselli et al., 2008;
68 Cavalli et al., 2013); or more recently, the coupling of conceptual models with probability theory
69 (Mahoney et al., 2020a, 2020b). In specific, the use of process-based soil erosion and sediment transport
70 models might be an important pathway to improve our understanding of sediment connectivity (Nunes



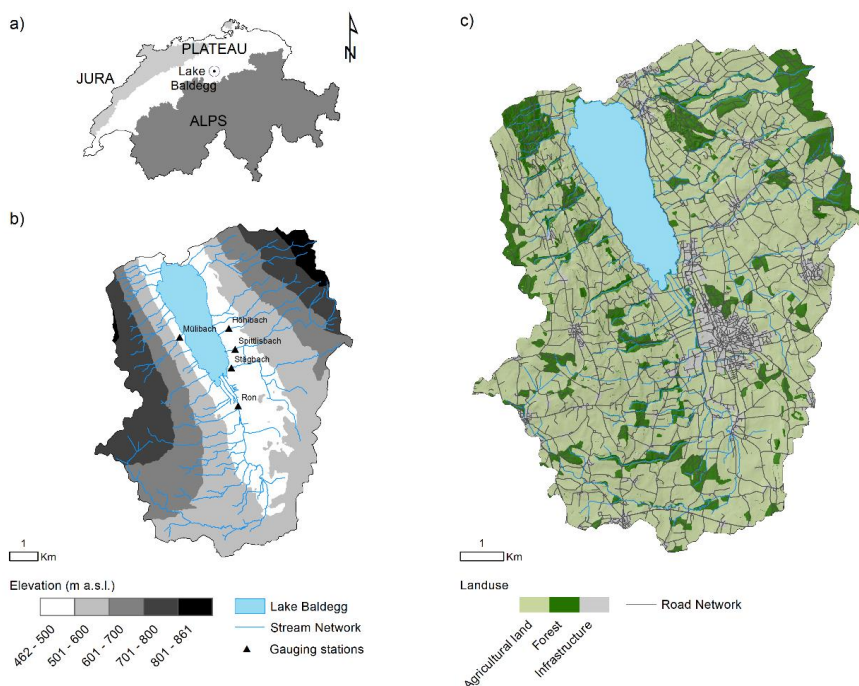
71 et al., 2018). However, erosion models in general, and process-based models in particular, face two
72 fundamental problems for representing sediment connectivity : (i) the input data requirements are large
73 and uncertain, and model application is often restricted to small catchments with a few square kilometres
74 (e.g. Baartman et al., 2020; Starkloff and Stolte, 2014; Wilken et al., 2017) and (ii) the implemented
75 process descriptions, especially along linear landscape features and field boundaries, are weakly defined
76 due to the aforementioned unavailability of experimental data. On the other hand, Borrelli et al. (2018)
77 demonstrated how parcel-specific high resolution land cover and management data can improve soil
78 erosion/sediment delivery models in patchy agricultural catchments.

79 Here, we aimed to (i) adapt a conceptual soil erosion and sediment delivery model with high spatial
80 resolution data (2 m x 2 m) within a Monte Carlo framework; (ii) to analyse the sediment connectivity
81 in a very patchy mesoscale catchment (73 km²) in Switzerland; and (iii) to perform a sensitivity analysis
82 of model parameters and structural assumptions regarding how linear features (dis)connect the sediment
83 cascade. Hence, we demonstrate how models can be used to understand the interaction between linear
84 features, landscape patchiness, and sediment connectivity. This will contribute to increase our
85 comprehension of relevant connectivity processes and our ability to develop appropriate measures for
86 reducing off-site erosion impacts.

87 **2 MATERIALS AND METHODS**

88 **2.1 Study catchment**

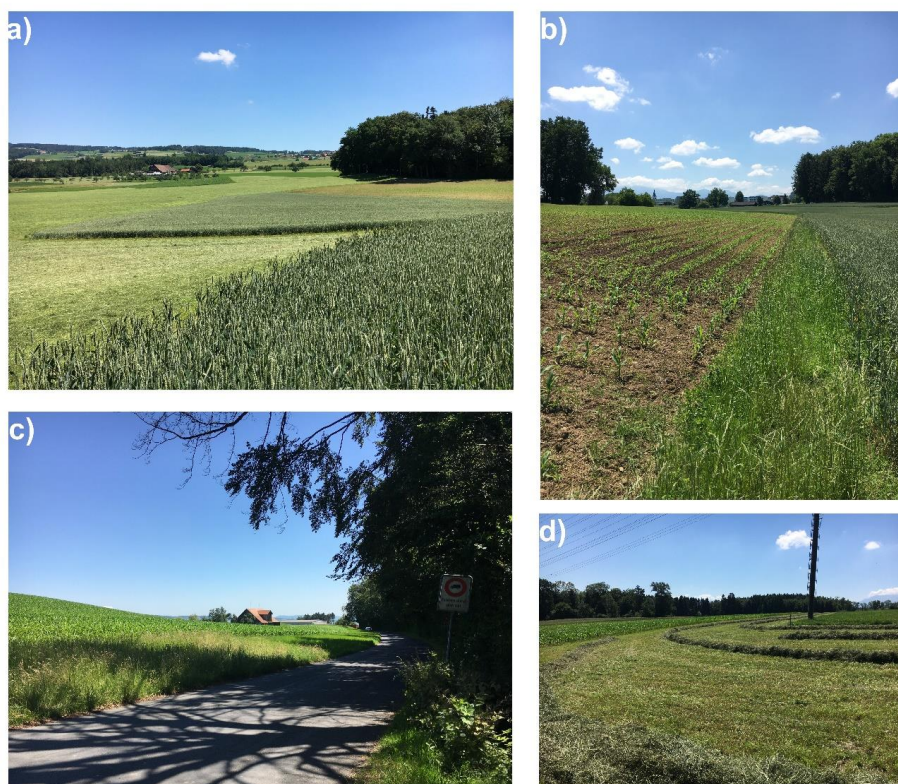
89 The study catchment consists of the contributing area of the Baldegg Lake, in the central Swiss Plateau
90 (Figure 1). The lake has been extensively studied due to its hypertrophic waters, which have been
91 artificially oxygenated since 1983 (e.g. Lavrieux et al., 2019; Müller et al., 2014; Teranes and
92 Bernasconi, 2005). The eutrophication of the lake has been mostly linked to excessive phosphorus loads
93 during the 20th century (Wehrli et al., 1997). Although water quality in the lake is currently improving
94 (BAFU, 2016), the supply of phosphorus-rich sediment is still a concern to local authorities (Stoll et al.,
95 2019). Hence, we chose to focus our study on the Baldegg catchment by reason of the ongoing research
96 in the area and the availability of comprehensive hydrological data, which has been monitored by the
97 department of environment and energy of Canton Luzern. Importantly, the catchment is representative
98 of the patchy agricultural landscape of the Swiss Plateau, as we detail below.



99

100 Figure 1. a) Location of the Lake Baldegg catchment; b) elevation, stream network, and location of
101 hydrological gauging stations; c) land use. Data source: Swisstopo, 2020.

102 The Baldegg catchment has a total area of 73.2 km², of which 5.2 km² are covered by the lake. The
103 remaining area is occupied by agricultural land (74%), forests (16%), and settlements (10%) (Swisstopo,
104 2020) (Figure 1c). The agriculture consists of intensively managed temporary pastures, cereal
105 production under crop rotation, permanent grasslands, fruit orchards, and small vineyards (Lavrieux et
106 al., 2019; Stoll et al., 2019). Agricultural field-blocks, here delimited by external boundaries (e.g. roads,
107 water courses, and forests) (Bircher et al., 2019), have a median size of 4.4 ha. However, smaller patches
108 separated by hedges, tree lines, and grass-buffer-strips, are generally found within the blocks (Figure 2).



109

110 Figure 2. Typical agricultural landscapes from the Baldegg catchment: a) Small arable and grassland
111 patches within larger field-blocks, b) Grass-buffer-strip between maize and wheat fields, c) wide grass-
112 buffer-strip between maize field and a vicinal road, d) freshly cut hay from a pasture in between maize
113 fields.

114 The road network density in the Baldegg catchment is 6.0 km km^{-2} , which is approximately three times
115 higher than the stream density (1.9 km km^{-2}). Streams in the upper catchment are often incised, with
116 visible, yet not prominent, signs of bank erosion. Flow is sometimes regulated in the lowland areas, and
117 tile drainage is found at water accumulation zones (Stoll et al., 2019). A total of 22 channels flow into
118 the Baldegg Lake, of which five streams are monitored for water and sediment discharge by cantonal
119 authorities, as described in section 2.2.

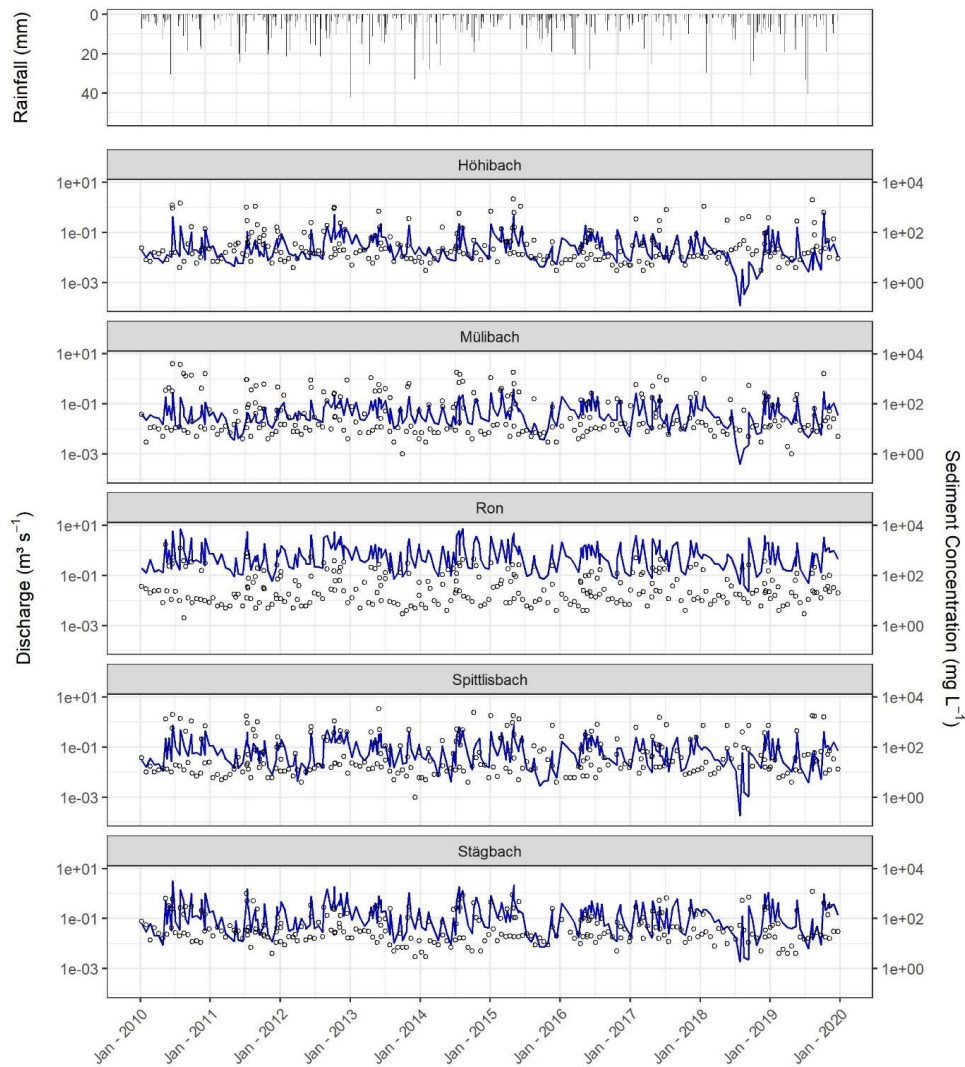
120 Elevation in the Baldegg catchment ranges from 462 to 861 m.a.s.l. Steeper slopes (maximum 35°) and
121 higher altitudes are found in the eastern and western sides of the catchment (Figure 1b), in a typical
122 glacial landscape of the Swiss Plateau – in this case formed by the retreat of the Reuss Glacier in the
123 south to north direction ($\sim 18,000$ years BP) (Keller, 2021; Pfiffner, 2021). As a result, calcareic



124 Cambisols developed upon Tertiary and Quaternary deposits are the main soil class in the catchment.
125 Rainfall is well distributed throughout the year, although greater precipitation is observed from May to
126 August. The average annual rainfall (2010-2020) at the closest gauging station is $\sim 1000 \text{ mm yr}^{-1}$
127 (Mosen, 454 m a.s.l., $\sim 3.5 \text{ km}$ north of the Baldegg lake, acquired from MeteoSwiss) and mean rainfall
128 erosivity in the catchment is $\sim 1150 \text{ MJ mm ha}^{-1} \text{ h}^{-1} \text{ yr}^{-1}$ (Schmidt et al., 2016).

129 **2.2 Tributary suspended sediment loads**

130 Suspended sediment concentrations from five tributaries flowing into the Baldegg Lake were measured
131 during ten years (Jan 2010 - Dec 2019) by the Department of Environment and Energy of Canton Luzern.
132 Approximately 275 grab samples were taken from each tributary, which corresponds roughly to two
133 samples per month, and high-flow events were opportunistically sampled (Figure 3). Suspended
134 sediments were measured at the same location where water discharge was monitored by automatic
135 gauging stations (Figure 1b). A summary of the measured rainfall, water discharge, and sediment
136 concentration from 2010 to 2020 is displayed in Figure 3.



137

138 Figure 3. Daily rainfall at the Mosen station, mean daily discharge (blue line), and sediment
139 concentration (circles) at the monitored tributaries of the Baldegg Lake (2010-2019).



140 In order to calculate the sediment load for the monitored tributaries, we fitted a rating curve (Equation
 141 1) with the measured sediment concentrations and their correspondent water discharge values.
 142 Additional covariates were included to account for hysteresis, seasonality, and constituent exhaustion
 143 (Table 1) (Vigiak and Bende-Michl, 2013; Wang et al., 2011):

$$\ln c_i = \beta_0 + \sum_{k=1}^5 \beta_k x_{k,i} + \varepsilon_i \quad (1)$$

144

145 Where: c is sediment concentration (mg L^{-1}) for day i , β_0 is the intercept, β_k are fitted coefficients, x_k are
 146 covariates (Tab. 1) accounting for discharge, hysteresis, seasonality and constituent exhaustion, and ε_i
 147 is the residual error.

148 Table 1. Covariates used for fitting the sediment-rating curve, as in Vigiak and Bende-Michl (2013) and
 149 Wang et al. (2011).

Covariate	Expression	Explanation	Physical interpretation
$x_{1,i}$	$\ln Q_i$	Q_i is = water discharge for day i (m^3s^{-1})	Discharge
$x_{2,i}$	$(\ln Q_i)^2$	Quadratic term of Q_i	Hysteresis
$x_{3,i}$	$\sin(2\pi M_i/12)$	M_i = month of day i	Seasonality
$x_{4,i}$	$\cos(2\pi M_i/12)$	M_i = month of day i	Seasonality
$x_{5,i}$	$\frac{\sum_{z=1}^i 0.95^{i+1-z} Q_z}{\sum_{z=1}^i 0.95^{i+1-z}}$	Discount flow up to day i	Constituent exhaustion (see Wang et al., 2011)

150

151 The rating curve was used to estimate daily sediment concentrations for the entire 2010-2020 period.
 152 Subsequently, we propagated the uncertainty in the regression fit by simulating posterior distributions
 153 of the model coefficients (β_0, β_k) with an informal Bayesian function of the R package ‘arm’ (Gelman
 154 and Hill, 2007), as in Batista et al. (2021). The posterior distributions were used to simulate 1000
 155 sediment concentration values for each day i . These were transformed into daily distributions of
 156 sediment loads (Mg), considering the mean daily discharge measurements from the gauging stations.
 157 Sediment loads were ultimately aggregated into average annual values (Mg yr^{-1}).

158 2.3 Model description

159 A modified version of the spatially distributed erosion and sediment transport WaTEM/SEDEM (Van
 160 Oost et al., 2000; Van Rompaey et al., 2001; Verstraeten et al., 2010) was used in this study.
 161 WaTEM/SEDEM provides a framework for modelling sediment connectivity from hillslope to water
 162 courses by use of a steady-state transport capacity equation and a pixel-based sediment routing
 163 component. That is, the model assumes that soil particles displaced by water erosion at a given grid-cell



164 are transferred downstream for as long as the runoff transport capacity is greater than the sediment
165 supply, or until the flow path reaches a definite sink. Although the model is able to simulate both tillage
166 and water erosion, here we focus on the latter, which is calculated with an adaptation of the RUSLE
167 (Renard et al., 1997):

168

$$A = R K L S_{2d} C P \quad (2)$$

169

170 Where: A is average annual soil loss ($\text{kg m}^{-2} \text{ yr}^{-1}$), R is rainfall erosivity ($\text{MJ mm m}^{-2} \text{ h}^{-1} \text{ yr}^{-1}$), K is soil
171 erodibility ($\text{kg h MJ}^{-1} \text{ mm}^{-1}$), $L S_{2d}$ is a topographic factor calculated by the Desmet and Govers (1996)
172 procedure (dimensionless), C is a cover-management factor (dimensionless), and P is a support practice
173 factor (dimensionless).

174 Transport capacity ($\text{kg m}^{-1} \text{ yr}^{-1}$) is assumed to be proportional to the potential to rill erosion, which is
175 described by a power function of slope length and gradient (Van Rompaey et al., 2001):

176

$$TC = K_{TC} R K (L S_{2d} - 4.12 S_g^{0.8}) \quad (3)$$

177

178 Where: K_{TC} is a landuse-dependent transport capacity coefficient (m) which requires calibration, R is
179 rainfall erosivity ($\text{MJ mm h}^{-1} \text{ yr}^{-1}$), K is soil erodibility ($\text{t h MJ}^{-1} \text{ mm}^{-1}$), $L S_{2d}$ is a topographic factor
180 calculated by the Desmet and Govers (1996) procedure (dimensionless), and S_g is slope gradient (m m^{-1}).
181

182 WaTEM/SEDEM partially incorporates the influence of the landscape structure on sediment transfer by
183 the use of a parcel connectivity parameter P_{Con} , which represents the proportion of sediment that is
184 stopped at field borders. The model also simulates runoff connectivity by means of a parcel trapping
185 efficiency P_{TEf} parameter, which corresponds to the proportion of the flow accumulation that is routed
186 downstream. Finally, the model is able to estimate the total amount of sediment transferred from
187 hillslopes to water courses, which can be interpreted as the hillslope component of a catchment sediment
188 budget. Since WaTEM/SEDEM does not represent channel erosion or in-stream deposition processes,
189 any comparison between modelled sediment yields and catchment-outlet sediment loads must be
190 interpreted with utmost caution. For further information on the model, we refer to Notebaert et al.,
191 (2006), Van Oost et al., (2000), Van Rompaey et al., (2001), and Verstraeten et al., (2010).

192 **2.4 Model implementation, input data, and sensitivity analysis**

193 WaTEM/SEDEM is usually implemented with a user-friendly GUI developed at KU Leuven, and freely
194 available at <https://ees.kuleuven.be/geography/modelling/watemsedem/>. Although the software



195 facilitates model application, it does not allow for more complex operations, such as sensitivity or
196 uncertainty analysis. Moreover, some model components might not be fully comprehensible without
197 access to the source-code, and WaTEM/SEDEM is frequently used as a black-box. Hence, in order to
198 perform a sensitivity analysis of model parameters and underlying structural model assumptions, we
199 implemented a WaTEM/SEDEM version using the free open source software R (R Core Team, 2021)
200 and SAGA GIS (Conrad et al., 2015). The main adaptations are described in the following, and our code
201 is available as supplementary material.

202 Our model application consists of a global all-at-a-time sensitivity analysis, as described by Pianosi et
203 al. (2016). That is, we performed a Monte Carlo simulation to explore the variability of the whole
204 parameter space, and all input factors were sampled simultaneously for each model realisation ($n =$
205 1200). The framework is similar to an uncertainty analysis, except in this case we did not focus on
206 quantifying uncertainty or locating the parameter space which produced behavioural model realisations.
207 Instead, we concentrated on apportioning sources of uncertainty to different model input factors (Pianosi
208 et al., 2016). This should allow us to identify parameters and model assumptions that have a greater
209 impact on the manner with which WaTEM/SEDEM describes sediment connectivity in the Baldegg
210 catchment.

211 For each iteration of the Monte Carlo simulation, all RUSLE input variables were sampled from uniform
212 distributions, except for the LS_{2d} factor (Table 2). Minimum and maximum R factor values were
213 retrieved from the Swiss national map (Schmidt et al., 2016), and a single lumped value for the whole
214 catchment was sampled for each iteration. The same approach was used for the K factor (Schmidt et al.,
215 2018). We used lumped catchment values for these factors due to their low spatial variability within the
216 study area, according to the national maps (coefficient of variations are 1% and 7% for the K and R
217 factor, respectively). For the C and P factors, here combined in a single CP parameter, uniform
218 distributions were created for each landuse class in the catchment, based on commonly used values from
219 the literature and a rasterised (2 m x 2 m) land cover map (1:25000) (Swisstopo, 2020). Due to the
220 unavailability of spatially distributed crop statistics in the Baldegg catchment, pastures and cropland
221 were aggregated into a single arable land category (Table 3). In this case, minimum and maximum values
222 were relaxed to represent a wide possible combination of crops and support practices. Such
223 combinations were assessed with the CP -Tool (Kupferschmied, 2019), which allows for the calculation
224 of CP values considering common crop rotation systems in Switzerland. Finally, the LS_{2d} factor was
225 calculated with a slope (rad) and an upslope contributing area (m^2) grid, which were obtained by
226 processing a 2 m x 2 m resolution DEM from SwissALTI3D (Swisstopo, 2014).



227 Table 2. Minimum and maximum parameter values sampled during the Monte Carlo simulation.

Parameter	Category	Min	Max
R (MJ mm m ⁻² h ⁻¹ yr ⁻¹)		950 10 ⁻⁴	1350 10 ⁻⁴
K (kg h MJ ⁻¹ mm ⁻¹)		0.025 10 ³	0.040 10 ³
CP	Arable land	0.01	0.5
	Grass-buffer-strips	0.001	0.009
	Forest	0.0001	0.003
	Orchard	0.001	0.2
	Vineyard	0.05	0.6
K_{TC} (m)	High	1	200
	Low	1	100
P_{TEf}		0	1
P_{Con}		0	1

228

229 Similarly, all WaTEM/SEDEM-specific model parameters were sampled from uniform distributions
 230 (Table 2). Landuse classes with a CP factor above 0.01 received higher transport capacity coefficients
 231 (K_{TC} high). The remaining landuse classes, namely forests and grass strips, received lower coefficients
 232 (K_{TC} low). The K_{TC} reference values were taken from Van Rompaey et al. (2001) and extended in order
 233 to explore a larger parameter space. The sampled parcel trapping efficiency (P_{TEf}) values were assigned
 234 to forests and grass-buffer-strips in the rasterised land cover map. The resulting P_{TEf} grid was used as a
 235 weight for calculating the aforementioned upslope contributing area. Hence, only a proportion of the
 236 grid-cell area from forests and grass-strips contributes to the downstream flow accumulation, as runoff
 237 amounts are assumed not to increase (or to increase slowly) with slope length under natural vegetation
 238 (Govers, 2011). Parcel connectivity (P_{Con}) values were assigned to the forest and grass-buffer-strips cells
 239 that bordered agricultural fields. The transport capacity (Eq. 2) at these cells was reduced by a fraction
 240 inversely proportional to the sampled P_{Con} value.

241 For each sampled combination of parameters values, the models were ran with and without the presence
 242 of grass-buffer-strips between agricultural field-blocks and adjacent roads and forests. Although grass-
 243 buffer-strips are generally present at field borders in the Baldegg catchment (Figure 2), these features
 244 were not distinguishable in the land cover map. Hence, we manually inserted 2 m wide grass-buffer-
 245 strips at the aforementioned borders. The extent of the buffer-strips in reality is quite variable, and
 246 generally wider at forest vicinities, as required by law in Switzerland (Alder et al., 2015). For simplicity,
 247 we used a single value that should allow us to test the sensitivity of the model to the presence of the
 248 strips. On the other hand, hedges and tree lines within field-blocks were already classified in the land
 249 cover map, and required no additional processing.

250 Furthermore, three road connectivity assumptions were assessed for each model iteration. In a first
 251 scenario, roads were treated as an ultimate sink, with zero transport capacity (i.e. ‘roads as sinks’).
 252 Hence, sediments reaching roads or infrastructure were subsequently removed from the system and did



253 not reach surface waters. This represents a scenario in which road and field drainage traps most
254 sediments and partly diverges runoff to wastewater treatment plants. A second scenario assumed that all
255 sediments reaching the road network were directly connected to the stream network. This represents a
256 situation in which the drainage system acts as a hydrological shortcut, transferring sediments from fields
257 into surface waters (i.e. ‘roads as shortcuts’) (see Schöenberger and Stamm, 2020). As in the original
258 model formulations (see Notebaert et al., 2006), the third scenario assigned very high transport capacity
259 to roads and infrastructure, so that no deposition would take place (i.e. ‘roads as patch-connectors’). In
260 this case, runoff and sediment might flow along or across the road network – which is expected to happen
261 during extreme rainfall events when the drainage system is clogged. Hence, sediment transfer will be
262 entirely dependent on the flow direction calculated from the DEM. Here we employed a multiple flow
263 direction algorithm, which was used for calculating upslope contributing area and routing sediments
264 along the flow-path. The sediment routing component was implemented with a capacity accumulation
265 function from SAGA GIS (Conrad et al., 2015). Of note, all geo-processing tools were applied with the
266 ‘RSAGA’ package (Brenning et al., 2018). Additional R packages essential to the simulations were
267 ‘doParallel’ (Ooi et al., 2019), ‘foreach’ (Calway and Weston, 2017), ‘raster’ (Hijmans, 2020), and
268 ‘rgdal’ (Binvand et al., 2019).

269 The sensitivity of WaTEM/SEDEM to the uncertainty in model parameters, the presence of grass-buffer-
270 strips, and assumptions about road connectivity was assessed by evaluating modelled hillslope sediment
271 yields (i.e., the amount of sediment delivered from hillslopes to surface waters) for the entire Baldegg
272 catchment. A qualitative analysis was performed with a visual inspection of scatter plots, comparing the
273 univariate parameter space with the model response surface. Additionally, we used a random forest
274 analysis to rank the importance of input factors to the uncertainty in model outputs (Antoniadis et al.,
275 2021). That is, a random forest predicted modelled sediment yields based on the sampled parameter
276 values in the Monte Carlo simulation. The importance of the input factors, including model parameters,
277 the presence of grass-strips, and the road connectivity scenarios, was ranked based on their relative
278 contribution to the RFA predictive error, following an out-of-bag estimate (Breiman, 2001). We chose
279 the RFA due to its ability to rank both qualitative and quantitative input factors. The analysis was
280 performed with the ‘randomForest’ (Liaw and Wiener, 2002) R package.

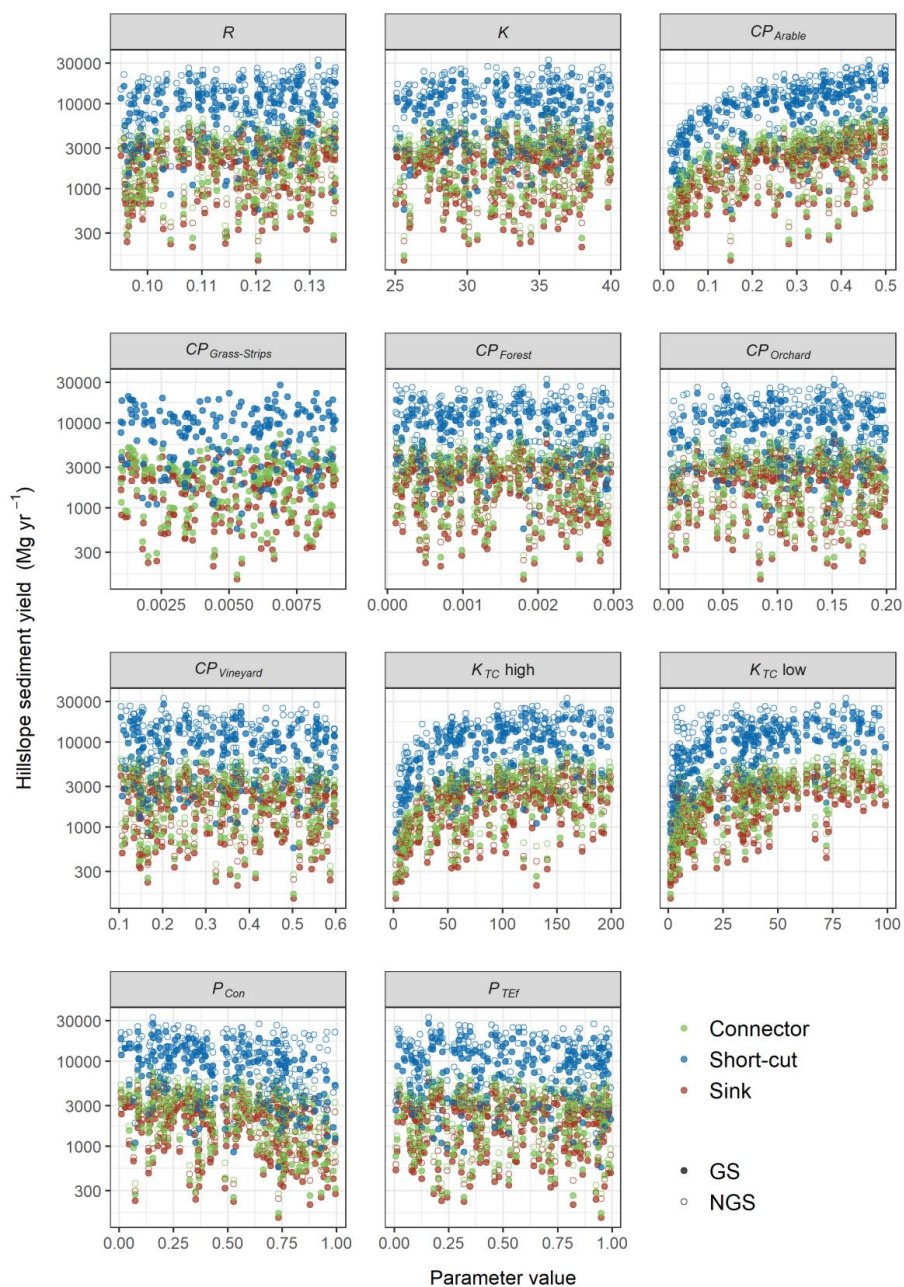
281 Finally, we compared the resulting WaTEM/SEDEM simulations of sub-catchment hillslope sediment
282 yields to the suspended sediment loads from the monitored tributaries. Of note, with this comparison we
283 only aim to provide a general picture of the plausibility of the model realisations. Suspended sediment
284 loads are a product of a complex interaction of hillslope and channel remobilisation processes, which
285 are not represented by WaTEM/SEDEM. Hence, modelled hillslope yields and suspended loads are not
286 fully commensurable, and we did not focus on a rejectionist framework for model testing. This research
287 is exploratory, and investigates the importance of linear features and landscape patchiness on sediment
288 connectivity.



289 **3 RESULTS**

290 **3.1 Sensitivity analysis**

291 The road connectivity assumptions were by far the most sensitive input factor for WaTEM/SEDEM in
292 the Baldegg catchment. This can be easily visualised in Figure 4, which presents scatter plots comparing
293 sampled parameter values and the model response surface. The uniformly scattered points denote a low
294 sensitivity of the modelled hillslope sediment yields to most input factors, with some evident exceptions:
295 *CP* for arable land, K_{TC} high, and K_{TC} low. On the other hand, all plots demonstrate that higher sediment
296 yields were calculated when we assumed that roads behaved as hydrological shortcuts, directly
297 connecting agricultural patches to the stream-network.

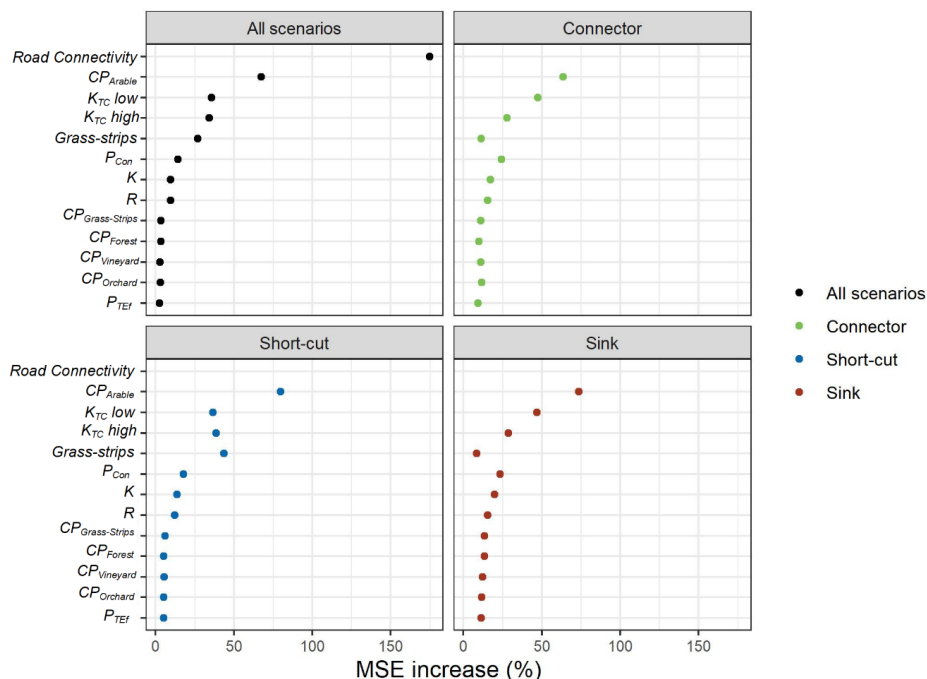


298

299 Figure 4. Univariate scatter plots of sampled parameter values. Full circles represent model realisations
 300 with the presence of grass-buffer-strips (GS), and open circles represent the ones without strips (NGS).
 301 Colours represent the road connectivity assumptions (i.e. ‘roads as patch-connectors’, ‘roads as
 302 hydrological shortcuts’, and ‘roads as sinks’). See section 2.4 for a description of road connectivity
 303 scenarios.



304 Similarly, the results from the RFA demonstrate that road connectivity was the most important input
 305 factor for predicting the WaTEM/SEDEM outputs (Figure 5). That is, if road connectivity was not
 306 considered, the mean-squared-error (MSE) increased in 175%. The MSE increase associated to *CP* for
 307 arable land (67.3%), K_{TC} low (35.6%), K_{TC} high (34.3%), and the presence of grass-buffer-strips
 308 (27.0%), indicate the model was also sensitive these input factors. However, if we considered each road
 309 connectivity scenario individually, the results from the random forest were shifted, as the model seemed
 310 to be more sensitive to the presence of grass-buffer-strips for the ‘road as shortcuts’ scenario (MSE
 311 increase = 43.6%).



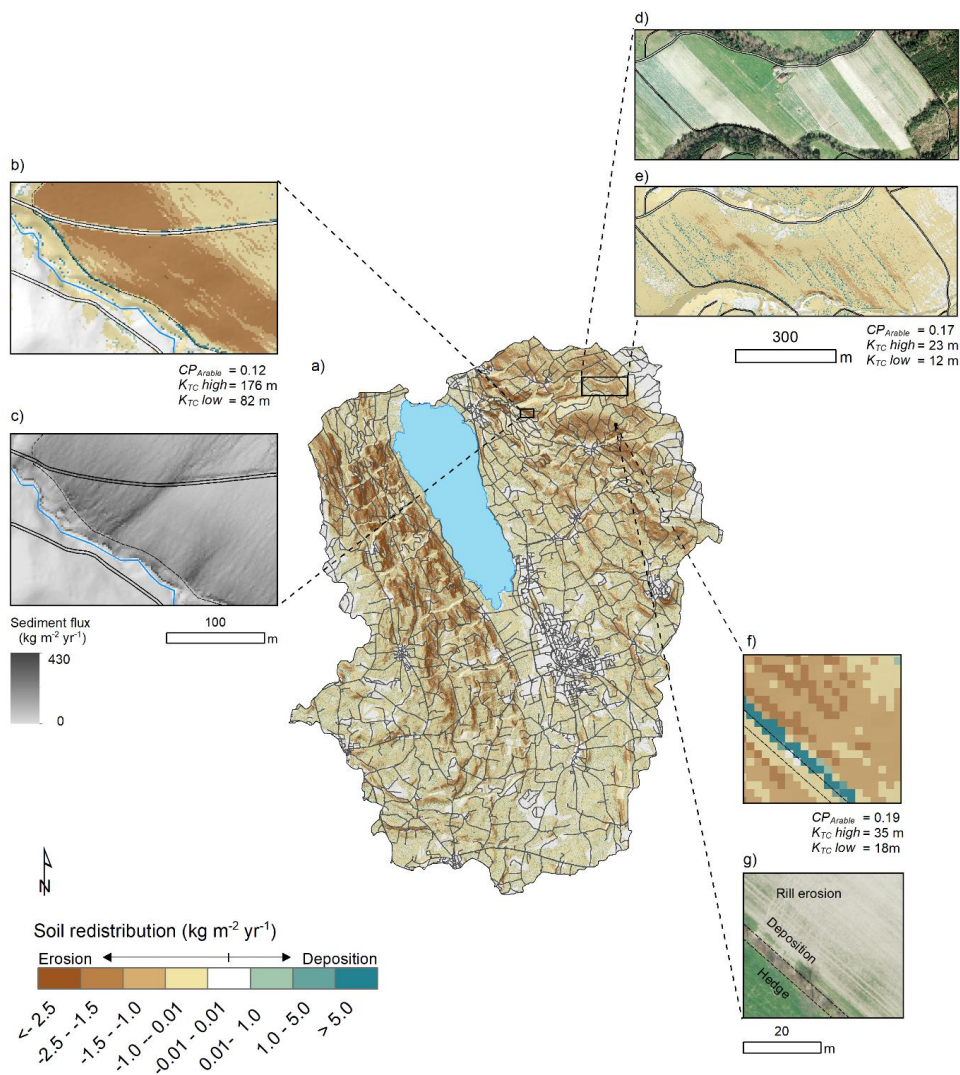
312

313 Figure 5. Mean-squared-error (MSE) increase associated to model input factors for the RFA. Larger
 314 relative errors indicate the input factors were more important for estimating model outputs.

315 3.2 Spatial patterns

316 The spatial patterns of soil redistribution rates were also highly influenced by linear features, landscape
 317 patchiness, and connectivity assumptions. Sediment deposition on field-blocks downslope from roads
 318 was more frequently observed for the ‘roads-as-connectors’ scenario, than for the other road
 319 connectivity assumptions. Specifically, when sediments were not diverged or trapped by the road
 320 network, there was a greater proportion of sediment deposition on foot-slope field borders and other
 321 potential sinks (Figure 6b).

322



323

324 Figure 6. a) Catchment patterns of soil redistribution for model a realisation with the presence of grass-
325 buffer-strips; b) detail of sediment deposition on field borders, 'road as patch connectors' scenario; c)
326 detail of sediment fluxes across the road network, 'road as patch connectors' scenario'; d) detail of aerial
327 image of multiple parcels within a field-block (SwissImage, 2014); e) soil redistribution rates for the
328 field-block; f) detail of sediment deposition at a grass-buffer-strip at a field border; g) aerial image for
329 the field (SwissImage, 2014).

330



331 The sediment flux from agricultural fields was generally interrupted when entering forest patches, and
 332 further deposition was modelled at forested valley floors, near the stream channels, for all scenarios
 333 (Figure 6b, c). Importantly, sediment deposition along grass-buffer-strips, hedges, and tree lines reduced
 334 sediment fluxes in between field-blocks, forming a patchy connectivity pattern. This was again visible
 335 for all simulated connectivity assumptions, albeit particularly pronounced when the presence of grass-
 336 buffer-strips was considered (Figure 6 a, f).

337 Unexpectedly, the soil redistribution patterns revealed that WaTEM/SEDEM simulated linear
 338 deposition areas at the borders of small cropland patches (Figure 6d, e). This occurred even in the
 339 absence of grass-buffer-strips or hedges, and hence without P_{Com} parameterisation, which was only
 340 applied to field-block borders. These depositional patterns were particularly evident within field-blocks
 341 oriented across the slope direction, and apparently stem from small-scale changes in the slope gradient,
 342 which were represented by the high-resolution DEM and which potentially results from long-term tillage
 343 erosion.

344 3.3 Soil redistribution rates, hillslope sediment-yields, and suspended sediment loads

345 Soil redistribution rates for eroding grid-cells in the Baldegg catchment were almost identical among
 346 the simulated road connectivity assumptions (Table 3). Higher absolute deposition rates were calculated
 347 for the simulations without grass-strips for both the connector and sink scenarios, which is a result of
 348 increased erosion rates calculated without the presence of the strips. On the other hand, lower sediment
 349 yields were calculated with the presence of grass-buffer-strips when the connectivity scenarios were
 350 analysed individually. Among these scenarios, deposition rates were lower if roads were considered to
 351 behave as hydrological shortcuts. Contrarily, deposition rates for the ‘roads as connectors’ and ‘roads
 352 as sinks’ scenarios were very similar, although road deposition was only modelled in the second case.
 353 Therefore, deposition rates within fields, patch-borders, colluviums, and valley-floors for the connector
 354 scenario were ~30% higher than for the other simulations. As the sediments not diverged by the road
 355 network were ultimately deposited within the catchment, the sink and connector scenarios displayed
 356 very similar hillslope sediment yields. Contrarily, sediment yields for the shortcut scenario were in
 357 general ~4.5 times higher than for the remaining road connectivity simulations.

358 Table 3. Summary statistics of soil redistribution rates, hillslope sediment yields calculated by the
 359 WaTEM/SEDEM simulations.

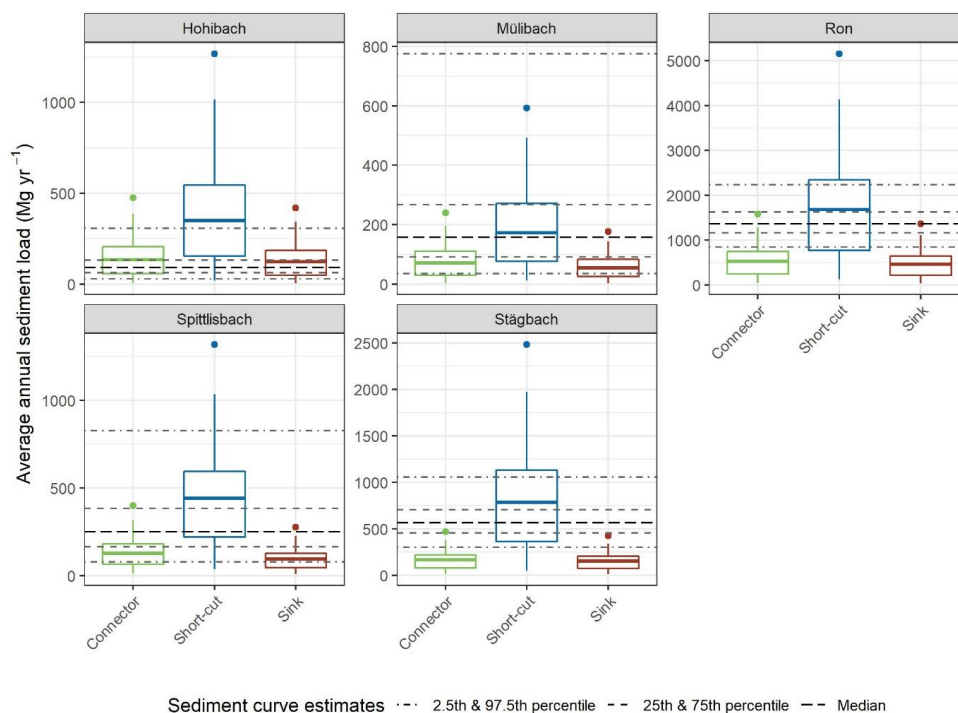
Scenario		Erosion			Deposition			SSY			SY		
		Mg ha ⁻¹ yr ⁻¹									Mg yr ⁻¹		
		Q1	Q2	Q3	Q1	Q2	Q3	Q1	Q2	Q3	Q1	Q2	Q3
Connector	GS	3.5	6.3	8.7	3.4	5.9	8.3	0.2	0.3	0.5	1,047	2,248	3,307
	NGS	3.7	6.6	9.1	3.5	6.1	8.5	0.2	0.4	0.6	1,498	3,054	4,097
Shortcut	GS	3.5	6.3	8.8	2.7	4.9	7.2	0.6	1.2	1.8	3,878	8,467	12,242
	NGS	3.7	6.6	9.2	2.5	4.7	6.7	0.9	1.9	2.6	6,303	13,238	17,506



Sink	GS	3.5	6.3	8.8	3.4	6.0	8.4	0.1	0.3	0.4	833	1,828	2,665
		NGS	3.7	6.6	9.2	3.5	6.2	8.7	0.2	0.4	0.5	1,143	2,389

360 SSY: area-specific hillslope sediment yield; SY: hillslope sediment yield. Deposition rates include
 361 hillslope and road deposition. GS: grass-buffer-strips; NGS: no grass-buffer-strips; Q1: first quartile, or
 362 the 25th percentile; Q2: second quartile, or the median; Q3: third quartile, or the 75th percentile.

363 The comparison between WaTEM/SEDEM simulations and the average annual loads from the
 364 monitored tributaries revealed a larger overlap between latter and the results from the ‘road-as-shortcuts’
 365 scenario (Figure 7). For this comparison, we only considered the simulations with the presence of grass-
 366 buffer-strips, which more closely represent the actual structure of the agricultural fields in the Baldegg
 367 catchment (see Figure 2). The overlap became particularly clear then we compared the interquartile
 368 range (IQR) of the calculations (Figure 7). That is, only a small proportion of the ‘road-as-connectors’
 369 and the ‘road-as-sinks’ model realisations encompassed the IQR of the tributary sediment loads, except
 370 for the Höhibach, which showed the opposite pattern.



371

372 Figure 7. Box-plots of hillslope sediment loads simulated by WaTEM/SEDEM for the road connectivity
 373 scenarios for each tributary sub-catchment. Dashed lines represent the percentiles of the sediment loads
 374 for each tributary, calculated based on the error propagation of the sediment-rating curve.

375 It is important to note that the median sediment concentrations calculated by the rating curve (Equation
 376 1) underestimated the actual observations, for all tributaries. This is expressed by the positive mean error

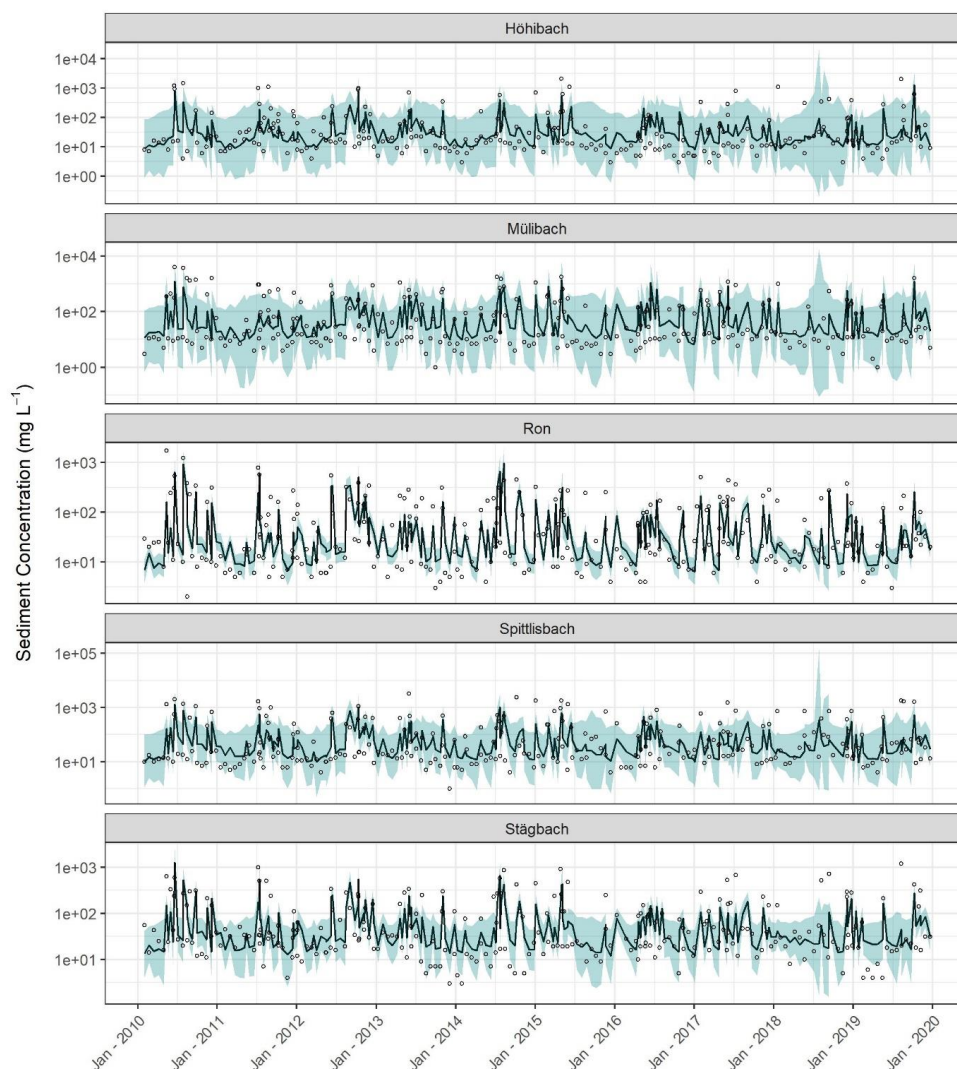


377 of the estimates (Table 4). Moreover, the Nash-Sutcliffe model efficiency coefficient for the median
378 calculations was unsatisfactory considering the usual thresholds for model performance (e.g. Moriasi et
379 al., 2015). On the other hand, the 95 % prediction interval of the rating curve encompassed a large
380 proportion of the observations, and most errors were associated to extreme events (Table 4, Figure 8).
381 Hence, it is likely that actual sediment loads from the tributaries are contained within the long right side
382 of the skewed distributions resulting from the error propagation of the rating curves (Figure 8).

383 Table 4. Evaluation metrics of the sediment rating curve, considering the measured sediment
384 concentrations and median of the simulations.

Stream	ME ----- mg L ⁻¹ -----	RSME	Out of bound percentage* ----- % -----	r _p	r _s	NSE
Höhibach	50.10	80.60	0.13	0.52	0.64	0.22
Mülibach	72.97	138.32	0.11	0.64	0.73	0.34
Ron	22.00	54.61	0.61	0.63	0.77	0.38
Spittlisbach	95.67	149.78	0.22	0.51	0.67	0.20
Stägbach	25.05	67.14	0.36	0.50	0.70	0.19

385 *percentage of observations out of the 95 % prediction interval. ME: mean error; RMSE: root-mean-
386 square error, r_p: Pearson's correlation coefficient, r_s: Spearman's correlation coefficient; NSE: Nash-
387 Sutcliffe model efficiency coefficient.



388

389 Figure 8. Log-scaled daily sediment concentrations estimates from the rating curve: dark solid line is
390 the median of the calculations and the shaded light blue represents the 95 % prediction interval. Open
391 circles are the observed values used for fitting the curve.

392 4 DISCUSSION

393 Here we assessed the interaction between landscape patchiness, linear structures, and sediment
394 connectivity. Our quantitative model-based approach highlighted the importance of roads in
395 (dis)connecting sediment fluxes between landscape compartments and surface waters in patchy
396 agricultural catchments, which are typical of the Swiss Plateau. These findings are very much in lines
397 with long-term field observations and qualitative model assessments for similar areas in Switzerland.



398 For instance, Ledermann et al. (2010) monitored off-site erosion in multiple fields from different regions
399 of the Swiss midlands, and found that linear features in general and roads in particular had a large
400 influence on runoff concentration, soil erosion rates, and off-site damage. These authors also estimated
401 that > 50 % of eroded soil was deposited in adjacent fields and infra-structure, while up to 20 % reached
402 surface waters, mainly through indirect inflow via the road and drainage network. Such figures are
403 proportionate to WaTEM/SEDEM estimations for the Baldegg catchment, specifically for the shortcut
404 scenario with the presence of grass-buffer-strips (Table 3). Another interesting similarity between our
405 outputs and the field assessments from Ledermann et al. (2010), was that both approaches identified
406 field border structures as critical regulators of soil erosion and sediment transport (see Figures 5 and 6).
407 According to the field assessments, border furrows are specifically important for both triggering erosion
408 and promoting diffuse sediment deposition. Such features, combined with long-term tillage erosion,
409 might be responsible creating the topographic pattern displayed in Figure 6d.

410 Moreover, the capacity of roads to connect runoff and sediments from arable land to surface waters in
411 Switzerland was extensively described by Alder et al. (2015) and Schönenberger and Stamm (2020).
412 Both studies used a similar semi-qualitative modelling approach for identifying agricultural fields that
413 were directly or indirectly (i.e. via the road and drainage networks) connected to surface waters. In
414 particular, Schönenberger and Stamm (2020) mapped the location of drainage inlets in multiple small
415 catchments of the Swiss Plateau. Accordingly, these authors identified the road drainage system as the
416 main hydrological shortcut connecting fields to water courses, as most drainage inlets discharge into
417 surface waters (87%), and only a small proportion of them flow into wastewater treatment plants or
418 depositional areas. Hence, the fact that the WaTEM/SEDEM ‘road as shortcuts’ scenario displayed a
419 greater agreement with the sediment rating curves for the Baldegg tributaries (Figure 7) is coherent with
420 the current understanding of runoff dynamics in the Swiss Plateau. Of note, the contrasting results for
421 the Höhibach sediment loads (Figure 7), which are much closer to the sink and patch-connector
422 simulations, do not seem to be explained by any physiographical specificity of the sub-catchment.
423 Hence, we speculate that this different pattern could be caused by a lower inlet drainage density in the
424 Höhibach sub-catchment, or by in-stream process, that are not accounted for in WaTEM/SEDEM.

425 In addition, our simulations of edge-of-field grass-buffer-strips indicated that these structures might be
426 particularly relevant for the ‘road as shortcuts’ scenario. In this case, the model estimated that grass-
427 strips could reduce up to 30% the sediment connectivity from hillslopes to surface waters in the Baldegg
428 catchment (Table 4). However, it should be noted that we assumed 2 m wide strips at field-block borders,
429 irrespectively of the adjacent structures or land use. As previously mentioned, the extent of these features
430 is in fact quite variable, and legislation only requires 0.5 m filters between fields and roads, as reported
431 by Alder et al. (2015). These authors further emphasised that albeit edge-of-field strips are an important
432 complementary management practice, their effectiveness is often reduced at high inflow areas, in which
433 very wide buffers would be necessary to stop sediment fluxes. Hence, Alder et al. (2015) recommended



434 that minimising on-site erosion rates was ultimately the most effective way to decrease sediment input
435 from arable land to water courses in Switzerland. Our results support this management proposition.
436 However, our simulations also indicate that the disproportional sediment connectivity afforded by the
437 dense road network translates into an excessive sediment supply to water courses, even when simulated
438 erosion rates were small. As on-site erosion rates in Switzerland are already reasonably low (see
439 Prasuhn, 2020), it might be important to consider solutions that address the sediment transport through
440 the underground drainage system, particularly in environmentally sensitive areas, such as the Baldegg
441 catchment.

442 In a wider context, our study has demonstrated how structural sediment connectivity patterns can be
443 investigated with a conceptual model as WaTEM/SEDEM, provided that model resolution is sufficiently
444 fine to represent relevant features and processes. In the Baldegg catchment, and likely in other patchy
445 agricultural landscapes, soil redistribution rates and patterns are intrinsically linked to linear features.
446 Hence, in order to provide relevant system descriptions, soil erosion models applied under similar
447 conditions must be able to represent linear features and landscape patchiness. Although these results
448 might seem case-specific, similar findings have been reported around the world. For instance, the effects
449 of roads and farm tracks in both coupling and decoupling runoff and sediments has been described in
450 Australia (Croke et al., 2005), Brazil (Bispo et al., 2020), Kenya (Stenfert Kroese et al., 2020), Italy
451 (Persichillo et al., 2018), and Spain (Calsamiglia et al., 2018). Moreover, the influence of linear features
452 such as field borders, hedges, terraces, and tractor tram lines in soil redistribution rates and patterns have
453 been well-documented in Europe (Calsamiglia et al., 2018b; Evrard et al., 2009; Fiener and Auerswald,
454 2005; Lacoste et al., 2014; Saggau et al., 2019), as well as the importance of landscape structure
455 (Baartman et al., 2020; Chartin et al., 2013; Fiener et al., 2011).

456 Another generalisable finding from our research was that WaTEM/SEDEM can be as sensitive to
457 RUSLE parameters as to the model-specific transport capacity coefficients. Therefore, when performing
458 uncertainty analyses of WaTEM/SEDEM, it is important to consider sources of error associated to the
459 RUSLE parameterisation. So far, uncertainty estimation methods applied to WaTEM/SEDEM have
460 focused on the K_{TC} parameterisation, and therefore have underestimated the uncertainty in model
461 predictions. We anticipate that our open-source WaTEM/SEDEM script will facilitate stochastic
462 implementations of the model, and ultimately promote uncertainty and sensitivity analysis of soil erosion
463 models. As recent studies have again demonstrated, results from soil erosion models are only
464 interpretable if the uncertainty in model structures, parameter estimation, and observational forcing data
465 are accounted for (Eekhout et al., 2021; Schürz et al., 2020).

466 5 CONCLUSIONS

467 Here we employed a global sensitivity analysis of the WaTEM/SEDEM model to investigate the
468 influence of linear structures and landscape patchiness on sediment connectivity in the Baldegg
469 catchment, a representative area of Swiss Plateau. In particular, this novel application of



470 WaTEM/SEDEM was implemented with the free programming language R, and our code is available as
471 supplementary material.

472 Our results demonstrated that assumptions about road connectivity were by far the most important factor
473 for modelling sediment transfer in the Baldegg catchment. Moreover, the comparison between extensive
474 model simulations and sediment rating-curve calculations indicated that roads behave as conduits for
475 sediment transport in the catchment. Hence, representing road connectivity is crucial for modelling
476 sediment transfer from hillslope to water courses in this agricultural catchment of the Swiss Plateau, and
477 potentially in other areas with a dense road drainage system. Moreover, our results further highlighted
478 the effects of linear structures and landscape patchiness on sediment connectivity. These findings were
479 made possible by the use of a model that was specifically tailored to explore the particularities of our
480 study area, by effectively exploring model assumptions and the parameter space, and by the use of high
481 resolution spatial data.

482 Overall, we found that WaTEM/SEDEM was useful for investigating sediment connectivity in the
483 Baldegg catchment, as it allowed us to unravel some of the processes and structures regulating hillslope
484 sediment transport in the area. If these processes and structures are accounted for, the model shows
485 potential for upscaling. In the case the model is be used for prediction and decision-making, we
486 recommend employing a fit-for-purpose rejectionist model testing framework, with multiple sources of
487 data, in order to evaluate the model's numerical accuracy and the quality of its spatial predictions.

488 **6 CODE AVAILABILITY**

489 The code for the model simulations was uploaded as a supplementary material file. If the manuscript is
490 accepted, we will upload the R script file and input data used for the simulations to the EnviDat platform
491 (<https://www.envidat.ch>).

492 **7 DATA AVAILABILITY**

493 If the manuscript is accepted, we will upload the input data used for the simulations to the EnviDat
494 platform (<https://www.envidat.ch>). This includes:

- 495 - Processed DEM
- 496 - Edited land cover rasters with the locations of grass buffer strips
- 497 - Road network map
- 498 - Field block map

499 The raw water discharge and sediment concentration data is property of the Department of Environment
500 and Energy of Canton Luzern, and can be shared upon their discretion.

501 **8 AUTHOR CONTRIBUTIONS**



502 PVGB and PF developed the model code, PVGB performed the simulations and analysed the data. SS
503 prepared model input data. PVGB prepared the manuscript with contributions from all authors. CA
504 revised the manuscript.

505 **9 COMPETING INTERESTS**

506 The authors declare no conflict of interest.

507 **10 ACKNOWLEDGEMENTS**

508 The authors would like to thank Robert Lovas, from the department of environment and energy of
509 Canton Luzern, who supplied the sediment concentration and water discharge monitoring data used in
510 this manuscript. We also appreciate the help from Axel Birkholz in acquiring the data. PVGB would
511 like to thank Franz Conen and Claudia Mignani for their multiple and valuable inputs regarding the
512 conceptualisation and preparation of this manuscript.

513



514 **REFERENCES**

- 515 Alder, S., Prasuhn, V., Liniger, H., Herweg, K., Hurni, H., Candinas, A. and Gujer, H. U.: A high-
516 resolution map of direct and indirect connectivity of erosion risk areas to surface waters in
517 Switzerland-A risk assessment tool for planning and policy-making, *Land Use Policy*, 48, 236–249,
518 doi:10.1016/j.landusepol.2015.06.001, 2015.
- 519 Antoniadis, A., Lambert-Lacroix, S. and Poggi, J. M.: Random forests for global sensitivity analysis:
520 A selective review, *Reliab. Eng. Syst. Saf.*, 206 (November 2020), 107312,
521 doi:10.1016/j.res.2020.107312, 2021.
- 522 Baartman, J. E. M., Nunes, J. P., Masselink, R., Darboux, F., Biellers, C., Degré, A., Cantreul, V.,
523 Cerdan, O., Grangeon, T., Fiener, P., Wilken, F., Schindewolf, M. and Wainwright, J.: What do
524 models tell us about water and sediment connectivity?, *Geomorphology*, 367, 107300,
525 doi:10.1016/j.geomorph.2020.107300, 2020.
- 526 BAFU: Faktenblatt: Der Greifensee, Zustand bezüglich Wasserqualität, 1–8 [online] Available from:
527 <http://www.bafu.admin.ch>, 2016.
- 528 Bakker, M. M., Govers, G., van Doorn, A., Quetier, F., Chouvardas, D. and Rounsevell, M.: The
529 response of soil erosion and sediment export to land-use change in four areas of Europe: The
530 importance of landscape pattern, *Geomorphology*, 98(3–4), 213–226,
531 doi:10.1016/j.geomorph.2006.12.027, 2008.
- 532 Batista, P. V. G., Lacey, J. P., Davies, J., Carvalho, T. S., Tassinari, D., Silva, M. L. N., Curi, N. and
533 Quinton, J. N.: A framework for testing large-scale distributed soil erosion and sediment delivery
534 models: Dealing with uncertainty in models and the observational data, *Environ. Model. Softw.*, 137,
535 doi:10.1016/j.envsoft.2021.104961, 2021.
- 536 Bauer, M., Dostal, T., Krasa, J., Jachymova, B., David, V., Devaty, J., Strouhal, L. and Rosendorf, P.:
537 Risk to residents, infrastructure, and water bodies from flash floods and sediment transport, *Environ.*
538 *Monit. Assess.*, 191(2), doi:10.1007/s10661-019-7216-7, 2019.
- 539 Bircher, P., Liniger, H. and Prasuhn, V.: Aktualisierung und Optimierung der Erosionsrisikokarte (
540 ERK2) Die neue ERK2 (2019) für das Ackerland der Schweiz, 2, 2019.
- 541 Bispo, D. F. A., Batista, P.V.G., Guimarães, D. V., Silva, M. L. N., Curi, N. and Quinton, J. N.:
542 Monitoring land use impacts on sediment production : a case study of the pilot catchment from the
543 Brazilian program of payment for environmental services, *Rev. Bras. Ciência do Solo*, 44, :e0190167,
544 2020.
- 545 Bivand, R. Keitt, T., Rowlingson, B., Pebesma, E., Sumner, M., Hijmans, R., Rouault, E., Warmerdam,
546 F., Ooms, J., Rundel, C.: Rgdal: bindings for the ‘Geospatial’Data Abstraction Library. R package



- 547 version 1.4-8, 2019.
- 548 Boardman, J.: A 38-year record of muddy flooding at Breaky Bottom: Learning from a detailed case
549 study, *Catena*, 189(January), 104493, doi:10.1016/j.catena.2020.104493, 2020.
- 550 Borrelli, P., Meusburger, K., Ballabio, C., Panagos, P. and Alewell, C.: Object-oriented soil erosion
551 modelling: A possible paradigm shift from potential to actual risk assessments in agricultural
552 environments, *L. Degrad. Dev.*, 29(4), 1270–1281, doi:10.1002/ldr.2898, 2018.
- 553 Borselli, L., Cassi, P. and Torri, D.: Prolegomena to sediment and flow connectivity in the landscape:
554 A GIS and field numerical assessment, *Catena*, 75(3), 268–277, doi:10.1016/j.catena.2008.07.006,
555 2008.
- 556 Breiman, L.: Random Forests, *Machine Learning*, 45, 5–32,
557 <https://doi.org/10.1023/A:1010933404324>, 2001
- 558 Brenning, A., Bangs, D., Becker, M.: RSAGA. R package version 1.3.0, 2018.
- 559 Calsamiglia, A., García-Comendador, J., Fortesa, J., López-Tarazón, J. A., Crema, S., Cavalli, M.,
560 Calvo-Cases, A. and Estrany, J.: Effects of agricultural drainage systems on sediment connectivity in a
561 small Mediterranean lowland catchment, *Geomorphology*, 318, 162–171,
562 doi:10.1016/j.geomorph.2018.06.011, 2018a.
- 563 Calsamiglia, A., Fortesa, J., García-Comendador, J., Lucas-Borja, M. E., Calvo-Cases, A. and Estrany,
564 J.: Spatial patterns of sediment connectivity in terraced lands: Anthropogenic controls of catchment
565 sensitivity, *L. Degrad. Dev.*, 29(4), 1198–1210, doi:10.1002/ldr.2840, 2018b.
- 566 Cavalli, M., Trevisani, S., Comiti, F. and Marchi, L.: Geomorphometric assessment of spatial
567 sediment connectivity in small Alpine catchments, *Geomorphology*, 188, 31–41,
568 doi:10.1016/j.geomorph.2012.05.007, 2013.
- 569 Chartin, C., Evrard, O., Salvador-Blanes, S., Hirschberger, F., Van Oost, K., Lefèvre, I., Daroussin, J.
570 and Macaire, J. J.: Quantifying and modelling the impact of land consolidation and field borders on
571 soil redistribution in agricultural landscapes (1954-2009), *Catena*, 110, 184–195,
572 doi:10.1016/j.catena.2013.06.006, 2013.
- 573 Conrad, O., Bechtel, B., Bock, M., Dietrich, H., Fischer, E., Gerlitz, L., Wehberg, J., Wichmann, V.
574 and Böhner, J.: System for Automated Geoscientific Analyses (SAGA) v . 2 . 1 . 4, doi:10.5194/gmd-
575 8-1991-2015, 2015.
- 576 Croke, J., Mockler, S., Fogarty, P. and Takken, I.: Sediment concentration changes in runoff pathways
577 from a forest road network and the resultant spatial pattern of catchment connectivity,
578 *Geomorphology*, 68(3–4), 257–268, doi:10.1016/j.geomorph.2004.11.020, 2005.



- 579 Desmet, P.J.J., Govers, G.: A GIS procedure for automatically calculating the USLE LS factor on
580 topographically complex landscape units, *J. Soil Water Conserv.*, 51, 427-433, 1996.
- 581 Eekhout, J. P. C., Millares-Valenzuela, A., Martínez-Salvador, A., García-Lorenzo, R., Pérez-Cutillas,
582 P., Conesa-García, C. and de Vente, J.: A process-based soil erosion model ensemble to assess model
583 uncertainty in climate-change impact assessments, *L. Degrad. Dev.*, 32, 2409–2422,
584 doi:10.1002/ldr.3920, 2021.
- 585 Evrard, O., Cerdan, O., van Wesemael, B., Chauvet, M., Le Bissonnais, Y., Raclot, D., Vandaele, K.,
586 Andrieux, P. and Bièdiers, C.: Reliability of an expert-based runoff and erosion model: Application of
587 STREAM to different environments, *Catena*, 78(2), 129–141, doi:10.1016/j.catena.2009.03.009, 2009.
- 588 Fiener, P. and Auerswald, K.: Measurement and modeling of concentrated runoff in grassed
589 waterways, *J. Hydrol.*, 301(1–4), 198–215, doi:10.1016/j.jhydrol.2004.06.030, 2005.
- 590 Fiener, P., Auerswald, K. and Van Oost, K.: Spatio-temporal patterns in land use and management
591 affecting surface runoff response of agricultural catchments-A review, *Earth-Science Rev.*, 106(1–2),
592 92–104, doi:10.1016/j.earscirev.2011.01.004, 2011.
- 593 Fiener, P., Wilken, F. and Auerswald, K.: Filling the gap between plot and landscape scale – eight
594 years of soil erosion monitoring in 14 adjacent watersheds under soil conservation at Scheyern,
595 Southern Germany, *Adv. Geosci. Discuss.*, (July), doi:adgeo-2019-4, 2019.
- 596 Fryirs, K.: (Dis)Connectivity in catchment sediment cascades: A fresh look at the sediment delivery
597 problem, *Earth Surf. Process. Landforms*, 38(1), 30–46, doi:10.1002/esp.3242, 2013.
- 598 Gelman, A. and Hill, J.: *Data Analysis Using Regression and Multilevel/Hierarchical Models*,
599 Cambridge University Press, New York., 2007.
- 600 Govers, G. Misapplications and misconceptions of erosion models, in: *Handbook of erosion*
601 *modelling*, edited by Morgan, R.P.C., Nearing, M.A., Blackwell Publishing Ltd., Chichester, 117-134,
602 2011.
- 603 Heckmann, T., Cavalli, M., Cerdan, O., Foerster, S., Javaux, M., Lode, E., Smetanová, A., Vericat, D.
604 and Brardinoni, F.: Indices of sediment connectivity: opportunities, challenges and limitations, *Earth-*
605 *Science Rev.*, 187 (December 2017), 77–108, doi:10.1016/j.earscirev.2018.08.004, 2018.
- 606 Hijmans, R.J.: Raster: Geographic analysis and modelling with raster data. R package version 3.4-5,
607 2020.
- 608 Keller, B: Lake Lucern and its spectacular landscapes, in: *Landscapes and landforms of Switzerland*,
609 edited by Reynard, E., Springer Nature Switzerland, Cham, Switzerland, 305-324, doi:
610 <https://doi.org/10.1007/978-3-030-43203-4>, 2021.



- 611 Krasa, J., Dostal, T., Jachymova, B., Bauer, M. and Devaty, J.: Soil erosion as a source of sediment
612 and phosphorus in rivers and reservoirs – Watershed analyses using WaTEM/SEDEM, *Environ. Res.*,
613 171 (January), 470–483, doi:10.1016/j.envres.2019.01.044, 2019.
- 614 Kupferschmied, P.: CP-Tool: Ein Programm zur Berechnung des Fruchtfolge- und
615 Bewirtschaftungsfaktors (CP-Faktor) der Allgemeinen Bodenabtragungsgleichung (ABAG), 2019.
- 616 Laceby, J. P., Batista, P. V. G., Taube, N., Kruk, M. K., Chung, C., Evrard, O. and Orwin, J. F.:
617 Tracing total and dissolved material in a western Canadian basin using quality control samples to
618 guide the selection of fingerprinting parameters for modelling, *Catena*, 200 (April 2020), 105095,
619 doi:10.1016/j.catena.2020.105095, 2021.
- 620 Lacoste, M., Michot, D., Viaud, V., Evrard, O. and Walter, C.: Combining ^{137}Cs measurements and a
621 spatially distributed erosion model to assess soil redistribution in a hedgerow landscape in
622 northwestern France (1960-2010), *Catena*, 119, 78–89, doi:10.1016/j.catena.2014.03.004, 2014.
- 623 Lavrieux, M., Birkholz, A., Meusburger, K., Wiesenberg, G. L. B., Gilli, A., Stamm, C. and Alewell,
624 C.: Plants or bacteria? 130 years of mixed imprints in Lake Baldegg sediments (Switzerland), as
625 revealed by compound-specific isotope analysis (CSIA) and biomarker analysis, *Biogeosciences*,
626 16(10), 2131–2146, doi:10.5194/bg-16-2131-2019, 2019.
- 627 Ledermann, T., Herweg, K., Liniger, H. P., Schneider, F., Hurni, H. and Prasuhn, V.: Applying
628 erosion damage mapping to assess and quantify off-site effects of soil erosion in Switzerland, *L.*
629 *Degrad. Dev.*, 21, 353–366, 2010.
- 630 Liaw, A. and Wiener, M.: Classification and regression by randomForest, *R News*, 2, 18-22, 2002.
- 631 Mahoney, D. T., Fox, J., Al-Aamery, N. and Clare, E.: Integrating connectivity theory within
632 watershed modelling part I: Model formulation and investigating the timing of sediment connectivity,
633 *Sci. Total Environ.*, 740, 140385, doi:10.1016/j.scitotenv.2020.140385, 2020a.
- 634 Mahoney, D. T., Fox, J., Al-Aamery, N. and Clare, E.: Integrating connectivity theory within
635 watershed modelling part II: Application and evaluating structural and functional connectivity, *Sci.*
636 *Total Environ.*, 740, 140386, doi:10.1016/j.scitotenv.2020.140386, 2020b.
- 637 Moriasi, D. N., Gitau, M. W., Pai, N. and Daggupati, P.: Hydrologic and water quality models:
638 Performance measures and evaluation criteria, *Trans. ASABE*, 58(6), 1763–1785,
639 doi:10.13031/trans.58.10715, 2015.
- 640 Müller, B., Gächter, R. and Wüest, A.: Accelerated water quality improvement during
641 oligotrophication in peri-alpine lakes, *Environ. Sci. Technol.*, 48(12), 6671–6677,
642 doi:10.1021/es4040304, 2014.
- 643 Notebaert, B., Vaes, B., Verstraeten, G., Govers, G.: WaTEM / SEDEM version 2006 Manual., 2006.



- 644 Nunes, J. P., Wainwright, J., Biielders, C. L., Darboux, F., Fiener, P., Finger, D. and Turnbull, L.:
645 Better models are more effectively connected models, *Earth Surf. Process. Landforms*, 43(6), 1355–
646 1360, doi:10.1002/esp.4323, 2018.
- 647 Ooi, H., Microsoft Corporation, Weston, S., Tenenbaum, D.: doParallel: Foreach Parallel Adaptor for
648 the ‘parallel’Package. R package version 1.0.15, 2019.
- 649 Parsons, A. J., Wainwright, J., Brazier, R. E. and Powell, D. M.: Is sediment delivery a fallacy? Reply,
650 *Earth Surf. Process. Landforms*, 34 (February), 155–161, doi:10.1002/esp, 2009.
- 651 Persichillo, M. G., Bordoni, M., Cavalli, M., Crema, S. and Meisina, C.: The role of human activities
652 on sediment connectivity of shallow landslides, *Catena*, 160 (August 2016), 261–274,
653 doi:10.1016/j.catena.2017.09.025, 2018.
- 654 Pfiffner, O.A.: The structural landscapes of Central Switzerland, in: *Landscapes and landforms of*
655 *Switzerland*, edited by Reynard, E., Springer Nature Switzerland, Cham, Switzerland, 159-172, doi:
656 <https://doi.org/10.1007/978-3-030-43203-4>, 2021.
- 657 Pianosi, F., Beven, K., Freer, J., Hall, J. W., Rougier, J., Stephenson, D. B. and Wagener, T.:
658 Sensitivity analysis of environmental models: A systematic review with practical workflow, *Environ.*
659 *Model. Softw.*, 79, 214–232, doi:10.1016/j.envsoft.2016.02.008, 2016.
- 660 Prasuhn, V.: Twenty years of soil erosion on-farm measurement: annual variation, spatial distribution
661 and the impact of conservation programmes for soil loss rates in Switzerland, *Earth Surf. Process.*
662 *Landforms*, doi:10.1002/esp.4829, 2020.
- 663 R Development Core Team, R: A language and environment for statistical computing, 2021.
- 664 Renard, K., Foster, G. R., Weesies, G. A., McCool, D. K. and Yoder, D. C.: *Predicting Soil Erosion by*
665 *Water: A Guide to Conservation Planning With the Revised Universal Soil Loss Equation (RUSLE)*,
666 1997.
- 667 Saggau, P., Kuhwald, M. and Duttmann, R.: Integrating soil compaction impacts of tramlines into soil
668 erosion modelling: A field-scale approach, *Soil Syst.*, 3(3), 1–28, doi:10.3390/soilsystems3030051,
669 2019.
- 670 Schmidt, S., Alewell, C., Panagos, P. and Meusburger, K.: Regionalization of monthly rainfall
671 erosivity patterns in Switzerland, *Hydrol. Earth Syst. Sci.*, 20(10), 4359–4373, doi:10.5194/hess-20-
672 4359-2016, 2016.
- 673 Schmidt, S., Ballabio, C., Alewell, C., Panagos, P. and Meusburger, K.: Filling the European blank
674 spot—Swiss soil erodibility assessment with topsoil samples, *J. Plant Nutr. Soil Sci.*, 181(5), 737–748,
675 doi:10.1002/jpln.201800128, 2018.



- 676 Schöenberger, U. and Stamm, C.: Hydraulic Shortcuts Increase the Connectivity of Arable Land
677 Areas to Surface Waters, *Hydrol. Earth Syst. Sci. Discuss.*, (September), 1–41, doi:10.5194/hess-
678 2020-391, 2020.
- 679 Schürz, C., Mehdi, B., Kiesel, J., Schulz, K. and Herrnegger, M.: A systematic assessment of
680 uncertainties in large-scale soil loss estimation from different representations of USLE input factors-a
681 case study for Kenya and Uganda, *Hydrol. Earth Syst. Sci.*, 24(9), 4463–4489, doi:10.5194/hess-24-
682 4463-2020, 2020.
- 683 Starkloff, T. and Stolte, J.: Applied comparison of the erosion risk models EROSION3D and LISEM
684 for a small catchment in Norway, *Catena*, 118, 154–167, doi:10.1016/j.catena.2014.02.004, 2014.
- 685 Stenfert Kroese, J., Batista, P. V. G., Jacobs, S. R., Breuer, L., Quinton, J. N. and Rufino, M. C.:
686 Agricultural land is the main source of stream sediments after conversion of an African montane
687 forest, *Sci. Rep.*, 10(1), 1–15, doi:10.1038/s41598-020-71924-9, 2020.
- 688 Stoll, S., Arb, C. von, Jorg, C., Kopp, S. and Prasuhn, V.: Evaluation der stark zur Phosphor-Belastung
689 des Baldeggersees beitragenden Flächen., 2019.
- 690 Teranes, J. L. and Bernasconi, S. M.: Factors controlling $\delta^{13}\text{C}$ values of sedimentary carbon in
691 hypertrophic Baldeggersee, Switzerland, and implications for interpreting isotope excursions in lake
692 sedimentary records, *Limnol. Oceanogr.*, 50(3), 914–922, doi:10.4319/lo.2005.50.3.0914, 2005.
- 693 Van Oost, K., Govers, G. and Desmet, P. J. J.: Evaluating the effects of changes in landscape structure
694 on soil erosion by water and tillage, *Landsc. Ecol.*, 15(6), 577–589, doi:10.1023/A:1008198215674,
695 2000.
- 696 Van Rompaey, A. J. J., Verstraeten, G., Van Oost, K., Govers, G. and Poesen, J.: Modelling mean
697 annual sediment yield using a distributed approach, *Earth Surf. Process. Landforms*, 26(11), 1221–
698 1236, doi:10.1002/esp.275, 2001.
- 699 Verstraeten, G., Van Oost, K., Van Rompaey, A. J. J., Poesen, J. and Govers, G.: Evaluating an
700 integrated approach to catchment management to reduce soil loss and sediment pollution through
701 modelling, *Soil Use Manag.*, 18(4), 386–394, doi:10.1111/j.1475-2743.2002.tb00257.x, 2010.
- 702 Vigiak, O. and Bende-Michl, U.: Estimating bootstrap and Bayesian prediction intervals for
703 constituent load rating curves, *Water Resour. Res.*, 49(12), 8565–8578, doi:10.1002/2013WR013559,
704 2013.
- 705 Wainwright, J., Turnbull, L., Ibrahim, T. G., Lexartza-Artza, I., Thornton, S. F. and Brazier, R. E.:
706 Linking environmental régimes, space and time: Interpretations of structural and functional
707 connectivity, *Geomorphology*, 126(3–4), 387–404, doi:10.1016/j.geomorph.2010.07.027, 2011.
- 708 Wang, Y. G., Kuhnert, P. and Henderson, B.: Load estimation with uncertainties from opportunistic



- 709 sampling data - A semiparametric approach, *J. Hydrol.*, 396(1–2), 148–157,
710 doi:10.1016/j.jhydrol.2010.11.003, 2011.
- 711 Wehrli, B., Lotter, A. F., Schaller, T. and Sturm, M.: High-resolution varve studies in Baldeggersee
712 (Switzerland): Project overview and limnological background data, *Aquat. Sci.*, 59(4), 285–294,
713 doi:10.1007/BF02522359, 1997.
- 714 Wilken, F., Fiener, P. and Oost, K. Van: Modelling a century of soil redistribution processes and
715 carbon delivery from small watersheds using a multi-class sediment transport model, , 113–124,
716 doi:10.5194/esurf-5-113-2017, 2017.
- 717